Supporting Information

Vidali et al. 10.1073/pnas.0901170106

SI Methods

RNAi Constructs. The RNAi system used in this work has been previously described (1). To generate coding sequence (CDS)-RNAi constructs, we amplified fragments within the formin homology (FH)2 domain of 8 formins. Most fragments were ≈200 bp. Within this 200-bp region, in a stretch of 150 bp, class I formins (For1)A and For1B are >87% identical. Therefore, we expect the For1B RNAi construct to target both For1A and For1B. The fragments were amplified directly from genomic DNA for For1 and For3, or from cDNA for For2. The constructs were concatenated using restriction sites incorporated into the PCR primers (Table S3), digested, ligated, and amplified again. The PCR products were cloned into pENTR/D-TOPO (Invitrogen) using the manufacturer's recommendations, and sequenced. The CDS-RNAi fragment was transferred to the destination vector pUGGi (1) using LR clonase (Invitrogen). The resulting construct was verified by restriction digest. To generate the class II- 5′ UTR-RNAi constructs, we identified the 5′ UTR of the For2 from the genomic sequence by determining the ATG (start) codon and amplifying 300 bp upstream from that region. The mRNA sequence of this region was verified in For2A by cDNA sequencing. The PCR products from For2A and For2B were ligated and reamplified as indicated above, and cloned in pENT-TOPO (For2A+B-5′ UTR-RNAi). Also, the individual fragments were separately cloned (For2A-5′ UTR-RNAi and For2B-5′ UTR-RNAi). All constructs were sequenced, and transferred into pUGGi (1) as described above.

Complementation Constructs. The complete genomic sequence of For2A was amplified from the ATG to the STOP codon and cloned into pENT-TOPO generating For2A-pENT. The full-length genomic For2A expression construct was generated by transferring, via LR clonase, the genomic For2A fragment to the destination vector pTHUbi-Gate (2) containing the maize ubiquitin promoter, generating FL-For2A. Positive clones were verified by restriction digest.

Two strategies were used to generate For2A coding sequence (cds) constructs. Direct amplification of the full-length cds by RT-PCR was not successful, presumably because of the highly GC-rich content of the For2A FH1 domain sequence. Therefore, we amplified each For2A domain [phosphatase tensin (PTEN), FH1, and FH2] separately, and used either traditional restriction enzyme-mediated ligations or multisite Gateway recombination from Invitrogen. The traditional approach generated For2Acds-pENT with no additional linker sequences, whereas the Gateway approach generated a construct with small linkers (21 bp) between each domain.

In the first strategy, the PTEN and FH2 domains were amplified from cDNA and cloned into pENT-TOPO generating PTEN-pENT and FH2-pENT. The FH1 domain, which is comprised of a single large exon, was amplified from genomic DNA and cloned into pENT-TOPO generating FH1-pENT. All constructs were sequenced before proceeding to generate the final cds construct. Two ligations in series were performed to generate For2Acds-pENT. First, a BssSI fragment from PTEN-pENT was ligated into a BssSI-digested FH1-pENT clone generating PTEN-FH1-pENT. Subsequently, an XhoI/AscI fragment from FH2-pENT was ligated into PTEN-FH1-pENT digested with XhoI/AscI generating For2Acds-pENT. For2Acds was transferred to the pTHUbi-gate destination vector using an LR clonase reaction.

We used the PTEN-pENT clone in an LR clonase reaction with pTHUbi-gate to generate the PTEN construct used in Fig. S4. We generated 2AFH1FH2-pENT clone by replacing the FH2-His from 2AFH1FH2-His-pENT (see below) with the FH2-STOP from For2Acds-pENT, using an XhoI/AscI digest. 2AFH1FH2-pENT was incubated with pTHUbi-gate in an LR reaction to generate the For2A FH1FH2 construct used in Fig. S4.

The multisite gateway strategy required generation of 3 entry constructs: PTEN-L1L4, 2AFH1-R4R3, and 2AFH2-L3L2. These constructs were generated by amplification with primers incorporating specific attB sites (Table S3) of the For2Acds-pENT clone. All fragments were then transferred to the appropriate DONR vectors using BP clonase following the manufacturer's recommendations. The final construct (P-2-2) was generated by an LR clonase reaction containing all 3 entry clones and the pTHUbi-gate destination vector. All final expression constructs were verified by restriction digests.

The multisite gateway system was used to generate the chimeric formin genes. First, the coding sequence of For1D was amplified from cDNA and cloned into pENT-TOPO to generate For1Dcds-pENT. This clone was used as a PCR template for the entry clones described below. Two entry clones stemming from the For1D gene were required: 1DFH1-R4R3 and 1DFH2-L3L2. These clones were generated by amplification with primers incorporating specific attB sites (Table S3) of the For1Dcds-pENT clone. All fragments were then transferred to the appropriate DONR vectors using BP clonase. The final constructs were generated by mixing the appropriate entry clones together with the pTHUbi-gate destination vector in an LR clonase reaction. P-1-1 uses PTEN-L1L4 + 1DFH1-R4R3 + 1DFH2-L3L2. P-1-2 uses PTEN-L1L4 + 1DFH1-R4R3 + 2AFH2-L3L2. P-2-1 uses PTEN-L1L4 + 2AFH1-R4R3 + 1DFH2-L3L2.

The 3XmEGFP Tagging System. We used multisite gateway cloning to generate For2A-3XmEGFP for transient expression, and for the allele replacement construct, For2A3XmEGFP-AR. For transient expression, we used the 2-fragment system, and for the allele replacement construct, we used the 4-fragment system. For the 2- and 4-fragment systems, we generated 3XmEGFP-L5L2 and 3XmEGFP-L5L4, respectively. The construction of these vectors is identical except for the primers (Table S3) used to generate the appropriate attB sites required for the BP clonase reactions. We introduced the A207K mutation, which eliminates EGFP dimer formation, in EGFP (pEGFP-C1 from Clontech) using site directed mutagenesis generating pmEGFP-C1. We amplified mEGFP with primers (Table S3) that incorporated the appropriate attB sites and an additional BamHI site resulting in mEGFP-L5L2 and mEGFP-L5L4. We amplified mEGFP from pmEGFP-C1 with BamHI and BglII sites incorporated into the primers (Table S3), and cloned this fragment into pGEM-Teasy (Promega) following the manufacturer's recommendations, generating mEGFP-pGEM. The BamHI/BglII fragment of mEGFP-pGEM was ligated into mEGFP-L5L2 or meGFP-L5L4 linearized with BamHI 2 times generating 3XmEGFP-L5L2 or 3XmEGFP-L5L4. The initial entry and pGEM clones were verified by sequencing, and the subsequent ligations were verified by restriction digests to ensure proper orientation of the multiple mEGFPs.

For2A-3XmEGFP. We amplified the For2A gene from For2A-pENT with primers that incorporated the appropriate attB sites

and removed the stop codon to generate For2AnoSTOP-L1L5. In a 2-fragment multisite LR reaction, we mixed For2AnoSTOP-L1L5 and 3XmEGFP-L5L2 entry clones with the pTHUbi-gate destination vector to generate For2A-3XmEGFP.

For2A-3XmEGFP-AR. We used the 4-fragment multisite gateway system to generate an allele replacement targeting construct that integrated 3XmEGFP in-frame and downstream of the For2A locus. We constructed 4 entry clones: For2A5′tar-L1R5, 3XmEGFP-L5L4, NOSZeo-R4R3, and For2A3′tar-L3L2. All primers (Table S3) used for these constructs incorporate the appropriate attB sites; 978 bp of the For2A gene were amplified from For2A-pENT. A fragment containing the NOS terminator and Zeocin resistance cassette was amplified from a vector containing a NOS terminator-Lox site-35S-Zeo-Lox site (3); 1,002 bp of the 3′ end of the For2A gene, downstream of the stop codon, were amplified from genomic DNA. All fragments were subjected to a BP clonase reaction. The construction of 3X-GFP-L5L4 was described above. The allele replacement construct was generated with an LR clonase reaction including all 4 entry clones and the destination construct pGEM-gate, which is the Gateway cassette cloned in pGEM-Teasy (Promega). SwaI sites were engineered into the 5′ and 3′ ends of the replacement cassette to dropout the replacement cassette for transformation into moss.

PTEN-GFP. We used multisite gateway to generate PTEN-GFP. PTEN was amplified from For2Acds-pENT with primers (Table S3) incorporating appropriate attB sites; mEGFP was amplified from pmEGFP-C1 with primers (Table S3) incorporating appropriate attB sites. These fragments were used in a BP clonase reaction with appropriate DONR vectors to generate the following entry clones: PTEN-L1R5 and mEGFP2-L5L2.

Constructs for Biochemical Analysis. The 1DFH1FH2 was amplified from For1Dcds-pENT with primers (Table S3) incorporating a 6XHis tag on the 3′ end and cloned into pENT-TOPO generating 1DFH1FH2His-pENT. The resulting entry clone was subjected to an LR reaction with the pDEST15 destination vector to generate GST-1DFH1FH2-His. The 2AFH2 was amplified from For2Acds-pENT with primers (Table S3) incorporating a 6XHis tag on the 3′ end and cloned into pENT-TOPO generating 2AFH2-His-pENT. The XhoI/AscI fragment from 2AFH2-His-pENT was ligated into 2AFH1-pENT digested with XhoI/AscI to generate 2AFH1FH2-His-pENT, which was subsequently transferred into pDEST15 with an LR reaction to generate GST-2AFH1FH2-His.

We amplified the For1D FH2 domain from 1DFH1FH2-pENT with a forward primer incorporating an XhoI site and the M13R primer. The product was cloned in pGEM-Teasy and subsequently digested with XhoI/AscI to remove the 1DFH2 domain. This fragment was cloned into 2AFH1FH2-His-pENT that had been digested with XhoI/AscI to remove the 2AFH2 domain. After ligation, 2AFH1-1DFH2-His-pENT was generated and then moved to pDEST15 with an LR reaction generating GST-2AFH1-1D-FH2-His. We amplified the For1D FH1 domain from 1DFH1FH2-pENT with M13F primer and a reverse primer incorporating an XhoI site. This PCR product was cloned into pGEM-Teasy, which was subsequently digested with NotI/XhoI to remove the 1DFH1 fragment, which was cloned into 2AFH1FH2-His-pENT that had been digested with NotI/XhoI to remove the 2A FH1fragment, generating 1DFH1-2AFH2-His-pENT. This clone was subjected to an LR reaction with pDEST15 to generate GST-1DFH1-2AFH2-His.

Moss (Pp) profilin was amplified from PRFA-pTHUbi (2) with primers incorporating NdeI and EcoRI sites (Table S3). This fragment was cloned into pGEM-Teasy and subsequently released by an NdeI/EcoRI digest. The released fragment was ligated into an NdeI/EcoRI digested pMW172 (4) generating PrfA-pMW.

Real-Time RT-PCR Analysis of Transient RNAi Plants. The 300–500 1-week-old plants lacking nuclear GFP were manually picked with a fine needle, and total RNA was extracted using the RNeasy Plant Mini Kit (Qiagen), followed by DNase I treatment according to the manufacturer's protocol. Complementary DNA was synthesized from 15 ng of total RNA by using SuperScript II Reverse Transcriptase (Invitrogen) and oligo(dT) following the manufacturer's protocol. Real-time PCR was performed in quadruplicate. All real-time PCRs used 0.25 ng of cDNA as template in a 20 μL of reaction using the Brilliant II SYBR Green QPCR Master Mix (Stratagene). The PCR conditions were as following: 95 °C for 10 min, followed by 50 cycles of 95 °C for 30 s, 56 °C for 50 s, and 72 °C for 40 s. The primer sets were designed to have similar amplification efficiencies and are listed in Table S3. The ubiquitin10 gene was used as an internal control for all reactions. Real-time PCRs were carried out in an Eppendorf Mastercycler ep Realplex^2 thermal cycler, and data were analyzed with the Realplex software 2.2.

Cell Wall and Nuclear Staining. To determine the number of nuclei per plant, cells were simultaneously stained with calcofluor (fluorescent brightener 28) and 4′,6-diamidino-2-phenylindole (DAPI). Plants undergoing active gene silencing were selected with a fine metal needle into a solution of 100 mM Pipes, pH 6.8, 0.1% Nonidet P-40, 1 μg/mL calcofluor, 0.1 μg/mL DAPI, 2% paraformaldehyde. After 30-min incubation, the plants were mounted in 20 μL of the same solution under a coverslip. The preparation was sealed with a melted 1:1:1 mixture of petroleum jelly, lanolin, and paraffin. Images were acquired with the DAPI settings and 40× zoom and a 5× lens on a stereo microscope (Leica MZ16FA) and a color camera (Leica DF300FX) using 36-bit RGB. When the plants were bigger than the camera field, several images were taken. Total nuclei per plant were counted manually from the blue channel of the images.

Growth Rate Determination. To measure growth rates, 1-week-old plants undergoing active gene silencing were identified by loss of nuclear GFP fluorescence. After 4 days in protoplast regeneration medium bottom agar (PRMB), transformed plants were selected with 15 μg/mL hygromycin for 2 days in PpNH4 medium [1.03 mM $MgSO_4$/1.86 mM KH_2PO_4/3.3 mM $Ca(NO_3)_2$/45 μM $FeSO_4$/9.93 μM H_3BO_3/220 nM $CuSO_4$/1.966 μM $MnCl_2$/231 nM $CoCl_2$/191 nM $ZnSO_4$/169 nM KI/103 nM Na_2MoO_4/2.72 mM diammonium tartrate] and 1 day in PpNO3 medium (PpNH4 lacking diammonium tartrate). A piece of cellophane containing the plant undergoing silencing was cut and inverted on an agar pad formed with 100 μL of Hoagland's medium [4 mM KNO_3/2 mM KH_2PO_4/1 mM $Ca(NO_3)_2$/89 μM Fe citrate/300 μM $MgSO_4$/9.93 μM H_3BO_3/220 nM $CuSO_4$/1.966 μM $MnCl_2$/231 nM $CoCl_2$/191 nM $ZnSO_4$/169 nM KI/103 nM Na_2MoO_4], 1% agar, 1% sucrose. The cellophane was removed by sliding it away leaving the plant on the agar pad. After adding 7 μL of liquid Hoagland's medium with 1% sucrose, a coverslip was carefully placed on top. The chamber was sealed as described above. Several cells from each plant continue to grow under these conditions. Time lapse movies at 5-min intervals were acquired for at least 2 h using 63× zoom and a 1× lens in a stereo microscope (Leica MZ16FA) and a color camera (Leica DF300FX) using 12-bit grayscale. Growth rates were calculated by measuring the position of the tip in the first and last images. Some preparations will undergo a small amount of drift, which was corrected by identifying a reference point in the background debris, and subtracting its position.

Image Acquisition and Morphometric Analysis of Transient RNAi Assay. Before image acquisition, the transformation plates were relabeled and randomized. Thus, images of silenced plants were acquired by a blinded observer. Plants were photographed at 63× zoom as 24-bit RGB color images with a CCD camera (Leica DF300FX) on a fluorescence stereomicroscope (Leica MZ16FA). Filter combinations were for chlorophyll and GFP combined, excitation 480/40, dichroic 505 long pass, emission 510 long pass. Exposure settings were maintained throughout an experiment. Plants without nuclear GFP signal were cropped from other plants and debris by using a free hand region of interest. The red channel of the color images corresponding to chlorophyll fluorescence was digitally separated. The resulting 8-bit image was manually thresholded, and the total area estimated, same values set for a whole experiment. Circularity, a morphometric parameter was evaluated: circularity is defined as $4\pi \cdot \text{area}/\text{perimeter}^2$. All image analysis was done using macros written for ImageJ (http://rsb.info.nih.gov/ij/); macros are available on request.

High-Resolution Imaging of Growing Moss Cells. Moss cells are highly sensitive to manipulation. On movement to a microscope slide for high-resolution imaging, moss cells generally stop growing for several hours. To solve this problem, we determined that moss tissue should be subcultured on PpNO3 medium for at least 3 days before transfer to an imaging chamber as described above. With these conditions, cells immediately grow on observation and continue to grow for several hours. They can be observed with the confocal microscope and high resolution optics. Bleaching and cell damage are minimized by using low laser levels (1–2%). These settings allow for repeated observations over extended periods of time without major changes in fluorescence and no observable detrimental effects to the cells.

1. Bezanilla M, Perroud PF, Pan A, Klueh P, Quatrano RS (2005) An RNAi system in Physcomitrella patens with an internal marker for silencing allows for rapid identification of loss of function phenotypes. *Plant Biol* 7:251–257.
2. Vidali L, Augustine RC, Kleinman KP, Bezanilla M (2007) Profilin is essential for tip growth in the moss Physcomitrella patens. *Plant Cell* 19:3705–3722.
3. Perroud PF, Quatrano RS (2008) BRICK1 is required for apical cell growth in filaments of the moss *Physcomitrella patens* but not for gametophore morphology. *Plant Cell* 20:411–422.
4. Way M, Pope B, Gooch J, Hawkins M, Weeds AG (1990) Identification of a region in segment 1 of gelsolin critical for actin binding. *EMBO J* 9:4103–4109.

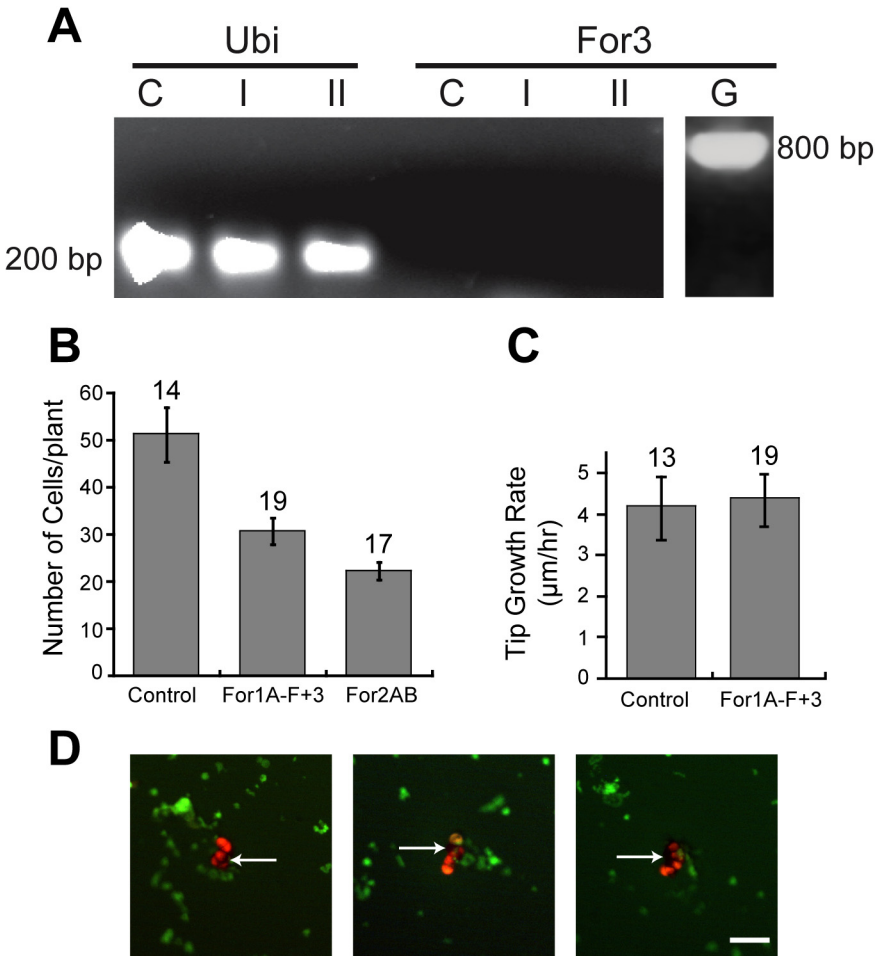

Fig. S1. (*A*) For3 is not expressed in protonemal tissue. RT-PCR analysis of 1-week-old plants undergoing silencing for the control (C), class I formins (I), and class II formins (II). PCR was performed on first-strand cDNA for 50 cycles. Ubi indicates RT-PCR product obtained with Ubiquitin 10 primers. For3 indicates RT-PCR performed with For3 primers. Note there is no amplification with the For3 primers. For3 primers are readily able to amplify from genomic DNA (G) using 35 cycles. (*B*) The number of cells per plant was quantified by staining 1-week-old plants with calcofluor and DAPI. The number of plants analyzed for each condition is indicated above the bars. (*C*) Tip growth rates for individual cells from 1-week old RNAi plants expressing either control or For1A-F+3 constructs were determined from time-lapse imaging. The number of cells analyzed for each condition is shown above the bars. (*D*) Fluorescent images of 1-week-old plants silencing all formins. Arrows indicate regions of dimming chlorophyll fluorescence. (Scale bar, 100 μm.)

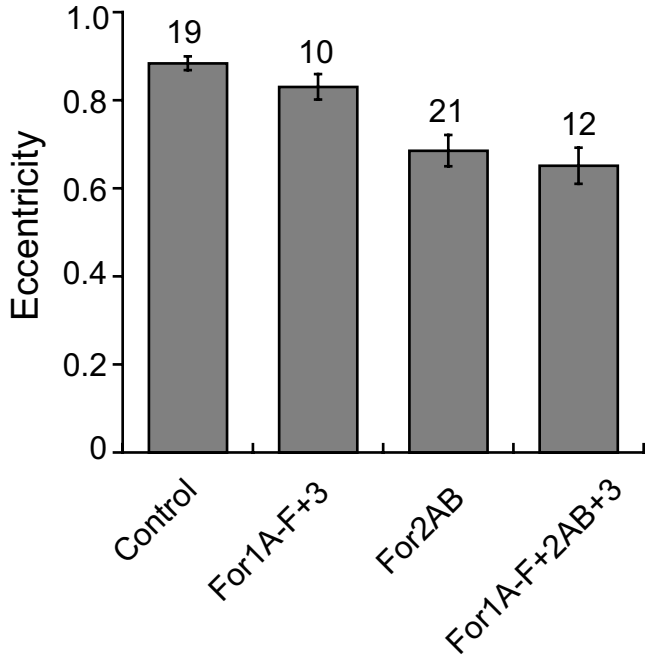

Fig. S2. Fast Fourier transform (FFT) analysis was performed on maximal projections from confocal Z-stacks of Alexa Fluor 488-phalloidin stained cells. Using a plug-in for ImageJ, an ellipse was fit to the central area of the FFT, and its eccentricity was calculated. A higher degree of axial orientation results in higher eccentricity (maximum value of 1), whereas disorganization results in lower eccentricity. Number of images analyzed is indicated above the bars.

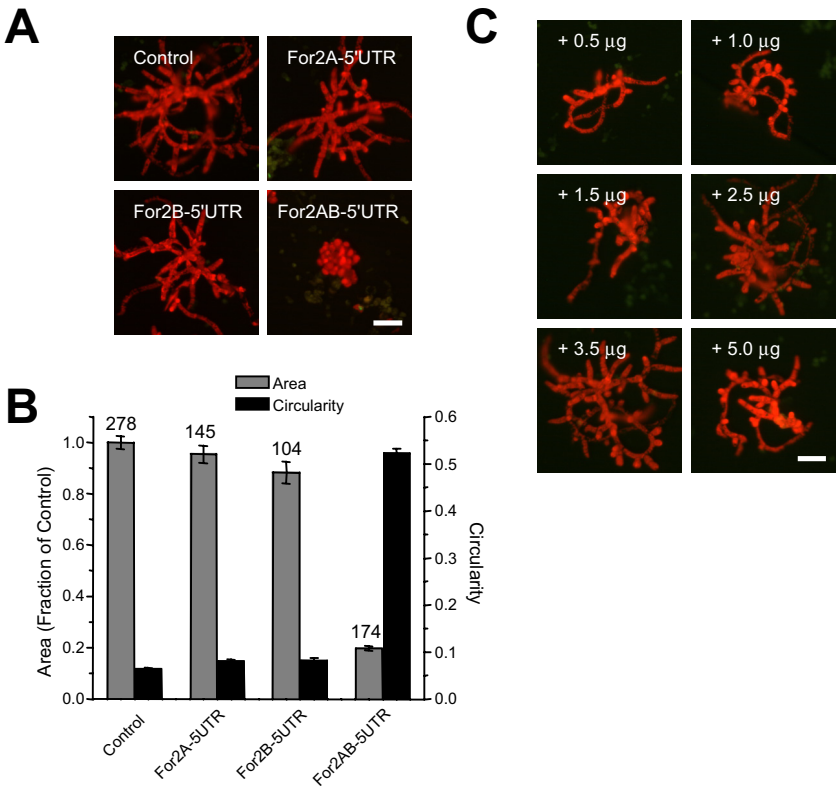

Fig. S3. A single For2 is sufficient for polarized growth. (*A*) Fluorescence micrographs of 1-week-old plants transformed with the indicated RNAi constructs. (Scale bar, 100 μm.) (*B*) Quantification of plant area (gray) and circularity (black) as described in Fig. 1. Error bars represent SEM. Numbers above the bars represent the total number of plants measured for each condition. (*C*) Fluorescence micrographs of 1-week-old moss plants transformed with For2AB-5′ UTR and increasing amounts in micrograms as indicated of For2Acds. (Scale bar, 100 μm.)

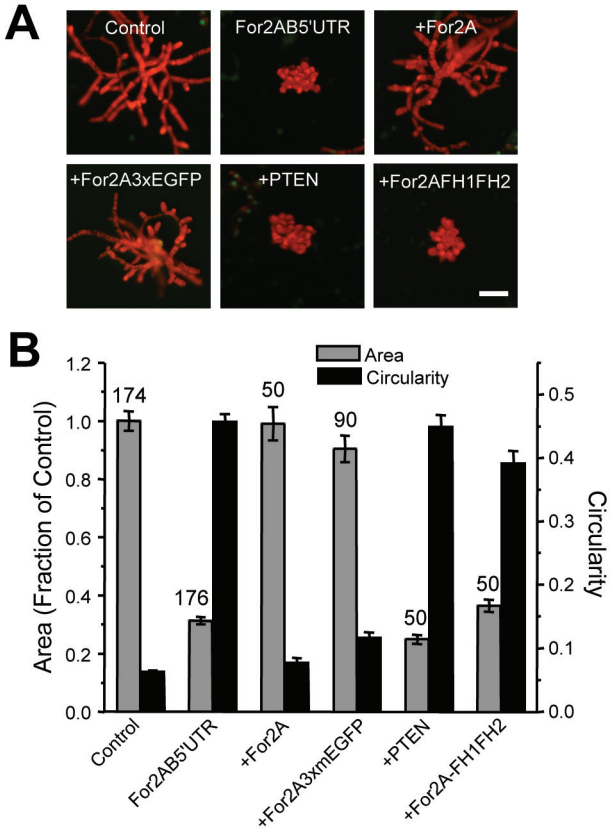

Fig. S4. Rescue of For2 RNAi. The full-length genomic clone of For2A with and without a C-terminal 3XmEGFP tag rescues the For2 RNAi phenotype. In contrast, the PTEN and FH1-FH2 domains alone are unable to rescue. (*A*) Representative fluorescence micrographs of 1-week-old moss plants, transformed with the indicated constructs. Panels labeled with + ''Construct'' are all transformed with For2AB-5′ UTR in addition to the construct indicated. (Scale bar, 100 μm.) (*B*) Quantification of plant area (gray) and circularity (black). Area is determined from the area of chlorophyll autofluorescence and is represented as a fraction of plants transformed with the control RNAi construct. Circularity is 4π·area/perimeter^2. Error bars represent SEM. Numbers above the bars represent the total number of plants measured for each condition.

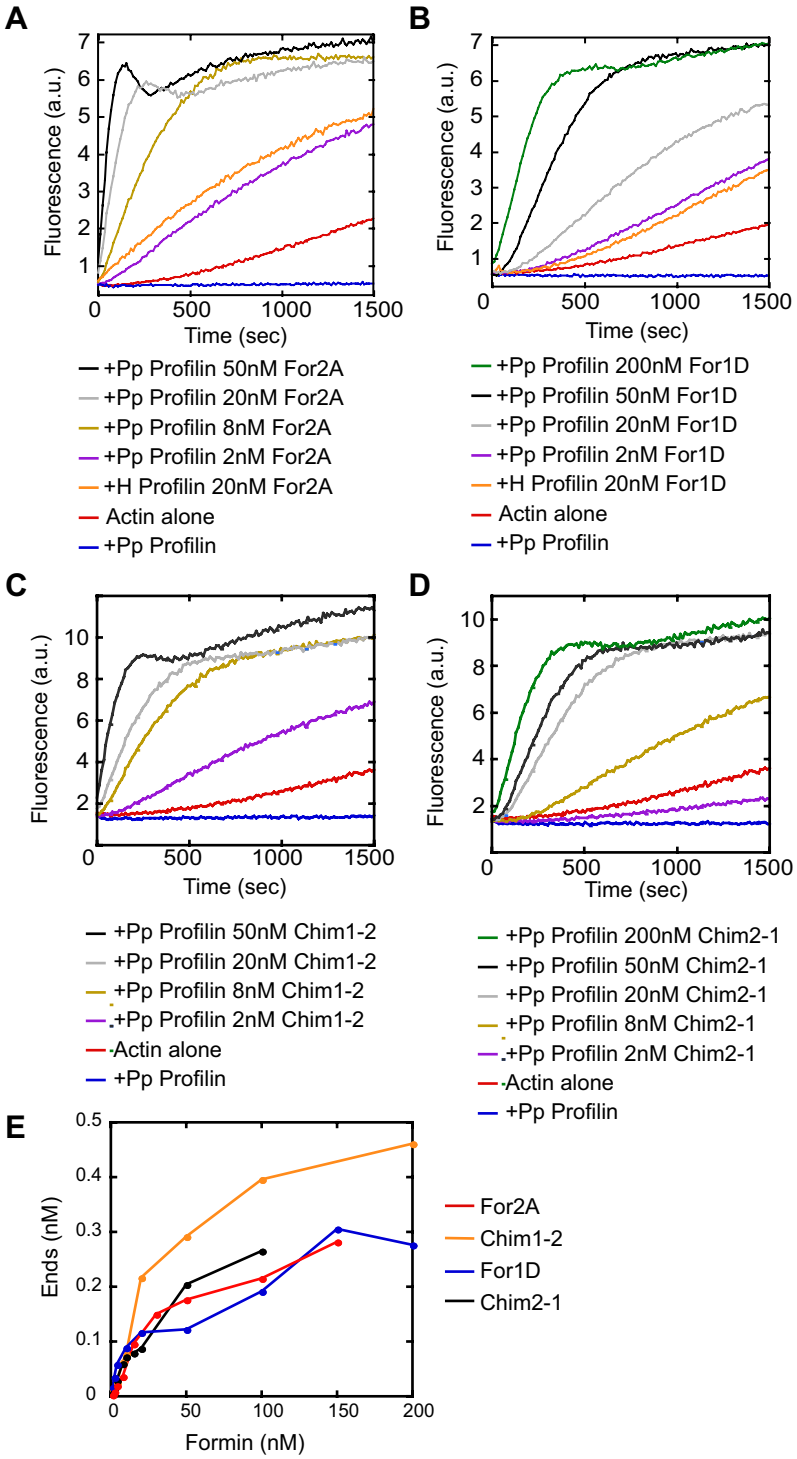

Fig. S5. For2A, For1D and the chimeric FH1-FH2 domains have similar actin nucleation efficiencies. (*A–D*) Rabbit muscle actin (2 μM, 10% pyrene-labeled) was assembled in the presence of the indicated concentrations of the FH1-FH2 domains of For2A (*A*), For1D (*B*), chim1-2 (*C*), or chim2-1 (*D*); 6 μM human (Hs) or moss (Pp) profilin was added as indicated. (*E*) Nucleation efficiency calculated from bulk experiments in *A–D* and elongation rates in Fig. 6.

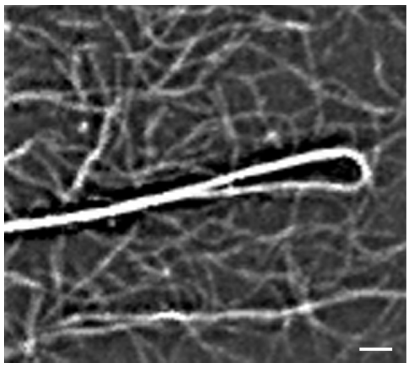

Fig. S6. TIRF image of actin filaments polymerized in the presence of Chim1-2. Note the large bundle of F-actin in the middle of the field. (Scale bar, 5 μm.)

Table S1. Statistical analyses from comparison of morphological parameters corresponding to Fig. 1

RNAi construct	For1A-C	For1DE	For1A-E	For1F + 3	For1A-F + 3	For2AB	For1A-F + 2AB + For3
				Area			
Control	0.1548	**0.0078**	**<0.0001**	**0.0008**	**<0.0001**	**<0.0001**	**<0.0001**
1A-C	—	0.9833	**0.0485**	0.7095	**<0.0001**	**<0.0001**	**<0.0001**
1DE	—	—	0.4113	0.9935	**0.0001**	**<0.0001**	**<0.0001**
1A-E	—	—	—	0.9385	0.3311	**<0.0001**	**<0.0001**
1F + 3	—	—	—	—	**0.0188**	**<0.0001**	**<0.0001**
1A-F + 3	—	—	—	—	—	**<0.0001**	**<0.0001**
2AB	—	—	—	—	—	—	**0.0095**
				Circularity			
Control	0.8092	**0.0479**	**<0.0001**	0.3552	**<0.0001**	**<0.0001**	**<0.0001**
1A-C	—	0.8428	**0.0129**	0.995	**<0.0001**	**<0.0001**	**<0.0001**
1DE	—	—	0.4682	0.9991	**<0.0001**	**<0.0001**	**<0.0001**
1A-E	—	—	—	0.2098	**0.0205**	**<0.0001**	**<0.0001**
1F + 3	—	—	—	—	**<0.0001**	**<0.0001**	**<0.0001**
1A-F + 3	—	—	—	—	—	**<0.0001**	**<0.0001**
2AB	—	—	—	—	—	—	0.0794

Adjusted *P* values are shown; values in bold indicate that the difference is statistically significant. Alpha level set at 0.05.

Table S2. Statistical analyses from comparison of morphological parameters corresponding to Fig. 4

RNAi construct	2AB-5′ UTR	+ P-2-2	+ P-2-1	+ P-1-1	+ P-1-2
			Area		
Control	**<0.0001**	**0.0003**	**<0.0001**	**<0.0001**	**<0.0001**
2AB-5′ UTR	—	**<0.0001**	0.4177	0.8938	0.994
+ P-2-2	—	—	**<0.0001**	**<0.0001**	**<0.0001**
+ P-2-1	—	—	—	0.9978	0.2077
+ P-1-1	—	—	—	—	0.7001
			Circularity		
Control	**<0.0001**	**<0.0001**	**<0.0001**	**<0.0001**	**<0.0001**
2AB-5′ UTR	—	**<0.0001**	**0.0003**	**<0.0001**	1.0000
+ P-2-2	—	—	**<0.0001**	**<0.0001**	**<0.0001**
+ P-2-1	—	—	—	0.769	0.2077
+ P-1-1	—	—	—	—	**<0.0001**

Adjusted *P* values are shown; values in bold indicate that the difference is statistically significant. Alpha level set at 0.05.

Table S3. Primers used in this study

Primer name	Primer sequence	Use
For1BRNAiF	CACCTGCAAGGAGCTGAAGGAAA	For1BC-CDS RNAi
For1BRNAiR	TACCGGATCCATAATCTCCTGTATGACGAAGTGAAG	For1BC-CDS RNAi
For1CRNAiF	TACCGGATCCTATTCCGAAAACTTCTAG	For1BC-CDS RNAi
For1CRNAiR	TACCGAATTCATCGAGCTAACCGAGCAATTTCTGAT	For1BC-CDS RNAi
For1DRNAiF	CACCGAATTCATTTACAAAGCTGCTGGAAGCAGTGT	For1DE-CDS RNAi
For1DRNAiR	TACCGGATCCTCTCAGTGATCACGAAGT	For1DE-CDS RNAi
For1ERNAiF-2	TACCGGATCCCCTTCACGAAACTGCTGG	For1DE-CDS RNAi
For5RNAiR	TACCCTCGAGCTTTGACGATCTCCTTGA	For1DE-CDS RNAi
For1FRNAiF	CACCCTCGAGGCATGCAAAGAGCTGAGA	For1F&3-CDS RNAi
For1FRNAiR	TACCGGATCCCAAAGTGCAACAAAGTGG	For1F&3-CDS RNAi
For3RNAiF	TACCGGATCCGCTTGCAATCAACTAAAATCAAGTC	For1F&3-CDS RNAi
For3RNAiR	TACCGAGCTCAAAATGGAGCAATGTGGTGTTCTTGT	For1F&3-CDS RNAi
For2ARNAiF	CACCGAGCTCAAGAATGGAAGCAAAGTTACGTGTG	For2AB-CDS RNAi
For2ARNAiR	TACCGGATCCCCTCTAGCAGTTCCTGAATTTAAG	For2AB-CDS RNAi
For2BRNAiF	TACCGGATCCGAGGATAGAAGCCAAGTTGCGTG	For2AB-CDS RNAi
Formin2B-R	CCTCGAGCTGTTCCAGAATTCA	For2AB-CDS RNAi
BamHIFor2A5UTR-F	CACCGGATCCTCTTTTGATGGATTGAACACACTCTATCAC	For2AB5′ UTR-RNAi
EcoRIFor2A5UTR-R	TACCGAATTCACTCCCATGCACGAAAGTATCAC	For2AB5′ UTR-RNAi
EcoRIFor2B5UTR-F	CACCGAATTCGCAGCCATTTGCGTATAGTGG	For2AB5′ UTR-RNAi
BamHIFor2B5UTR-R	TACCGGATCCATTCCCATGCACAAAGGTATCAC	For2AB5′ UTR-RNAi
For2AFL-CDS-F	CACCATGTCTCTGTTTCGCCGATTCTTC	For2A-pENT and PTEN-pENT
For2AFL-CDS-R	CTATCCAATCCTAGATCTCAATGGAGAAAATC	For2A-pENT and FH2-pENT
For2APTENattB4	GGGGACAACTTTGTATAGAAAAGTTGGGTGGCGATCACGAGATGAACT	PTEN-pENT and PTEN-L1L4
For2A-CACC-link-F	CACCGCCAACTCAGTGCTTCTGAGTTCATCTCGTGAT	FH1-pENT
For2A-FH2R2	TTTCTGATAATCGGCCCACAGACTCC	FH1-pENT
For2AXhoFH1FH2-F	CACCCTCGAGCTCCTGCTCCAGTGGCCGCACCAGTAATAAAGAAACCGGC-ACCCCTGAAACC	FH2-pENT and 2AFH2-His-pENT
For2APTENattB1	GGGGACAAGTTTGTACAAAAAAGCAGGCTTAATGTCTCTGTTTCGCCGA	PTEN-L1L4
For2AFH1attB3r	GGGGACAACTTTATTATACAAAGTTGTCTTTATTACTGGTGCGGC	For2AFH1-R4R3
For2AFH1attB4r	GGGGACAACTTTTCTATACAAAGTTGCTCCTAGCGGTGCTGCACCC	For2AFH1-R4R3
For2AFH2attB2	GGGGACCACTTTGTACAAGAAAGCTGGGTACTATCCAATCCTAGATCT	For2AFH2-L3L2
For2AFH2attB3	GGGGACAACTTTGTATAATAAAGTTGCTAAACCGGCACCCCTGAAA	For2AFH2-L3L2
PpFOR1D-F	CACCATGTCAAATTCGACGGTGGAG	For1Dcds-pENT
PpFor1D-R	TCAATTCGTTTTATTCGGCAGGG	For1Dcds-pENT
attB4rFor1DFH1Long	GGGGACAACTTTTCTATACAAAGTTGCT CCCCCTTCCACTCCTCCT	For1DFH1-R4R3
attB3rFor1DFH1	GGGGACAACTTTATTATACAAAGTTGT TATCAATGGAGCCAGCTT	For1DFH1-R4R3
attB3For1DFH2	GGGGACAACTTTGTATAATAAAGTTGCT TTACCTGCAAGACCTGATCT	For1DFH2-L3L2
attB2For1DFH1FH2-STOP	GGGGACCACTTTGTACAAGAAAGCTGGGTATCAATTCGTTTTATTCGGCAG	For1DFH2-L3L2
EGFPmonF	CCTGAGCACCCAGTCCAAGCTTAGCAAAGACCCCAAC	Site-directed mutagenesis of EGFP
EGFPmonR	GTTGGGGTCTTTGCTAAGCTTGGACTGGGTGCTCAGG	Site-directed mutagenesis of EGFP
attB5BamHmEGFP	GGGGACAACTTTGTATACAAAAGTTGTGGGATCCATGGTGAGCAAG-GGCGAG	mEGFP-L5L2 and mEGFP-L5L4
attB2mEGFPBgl	GGGGACCACTTTGTACAAGAAAGCTGGGTAAGATCTTTACTTGTACAGCT-CGTCCATGCC	mEGFP-L5L2
attB4mEGFP	GGGGACAACTTTGTATAGAAAAGTTGGGTGTTACTTGTACAGCTCGTC	mEGFP-L5L4
EYFPF	AATGGGATCCATGGTGAGCAAGGGCGAG	mEGFP-pGEM
EYFPR	AATGAGATCTCTTGTACAGCTCGTCCATGC	mEGFP-pGEM
For2AFLBPB1	GGGGACAAGTTTGTACAAAAAAGCAGGCTTAATGTCTCTGTTTCGCCGA	For2AnoSTOP-L1L5
For2AFLBPB5r	GGGGACAACTTTTGTATACAAAGTTGTTCCAATCCTAGATCTCAA	For2AnoSTOP-L1L5
attB1For2A-SwaI_1kb	GGGGACAAGTTTGTACAAAAAAGCAGGCTTAATTTAAATTTGGCTGAAG-AAATGCAAGCAGTT	For2A5′tar-L1R5
attB5rFor2A-NoStop_1kb	GGGGACAACTTTTGTATACAAAGTTGTTCCAATCCTAGATCTCAA	For2A5′tar-L1R5
AttB4r_nos_zeo_F	GGGGACAACTTTTCTATACAAAGTTGCGTTCAAACATTTGGCAATAAAGTT-TCTTAAGATTGAATCC	NOSZeo-R4R3
Nos_Zeo_attB3r_R	GGGGACAACTTTATTATACAAAGTTGTGGGCGAATTGGGCCCGACG	NOSZeo-R4R3
attB3For2A_1kb	GGGGACAACTTTGTATAATAAAGTTGCTGGCCTTCAAGTCACTTAT	For2A3′tar-L3L2
attB2For2A-SwaI_1kb	GGGGACCACTTTGTACAAGAAAGCTGGGTAATTTAAATCTGGTTTAAGCT-TTAAGC	For2A3′tar-L3L2
For2APTENattB1	GGGGACAAGTTTGTACAAAAAAGCAGGCTTAATGTCTCTGTTTCGCCGA	PTEN-L1R5
For2APTENB5rR	GGGGACAACTTTTGTATACAAAGTTGTGCGATCACGAGATGAACT	PTEN-L1R5
attB5-mEGFP-STOP-f	GGGGACAACTTTGTATACAAAAGTTGTGGTGAGCAAGGGCGAGGAG	mEGFP2-L5L2
attB2-mEGFP-STOP-r	GGGGACCACTTTGTACAAGAAAGCTGGGTATTACTTGTACAGCTCGTCCA-TGCC	mEGFP2-L5L2
For1D-FH1-Long-F	CACCGCCAATGCAGCTTTGCACAACCCTACT	1DFH1FH2His-pENT

Primer name	Primer sequence	Use
For1D-6His-R	CTAATGGTGATGGTGATGGTGATTCGTTTTATTCGGCAGGGAG	1DFH1FH2His-pENT
For2A-6His-R-NEW	CTAATGGTGATGGTGATGGTGTCCAATCCTAGATCTCAATGGAGA	2AFH2-His-pENT
XhoIFH21F	CTCGAGTACCTGCAAGACCTGATCTGGG	2AFH1–1DFH2-His-pENT
XhoIFH11R	CTCGAGTCAATGGAGCCAGCTTCGGAATC	1DFH1–2AFH2-His-pENT
PRFaNdeIExpF	CATATGTCTTGGCAATCGTACATCG	PrfA-pGEM
PRFaEcoRIExpR	GAATTCTCAAATTCCCTGTTCGTATAGG	PrfA-pGEM
For1A RT-F	GAAGCAGCAATGGAGAATCC	Real-time RT-PCR
For1A RT-R	TCTGCAAGTGCACCAATACG	Real-time RT-PCR
For1B RT-F	AAGGCCCAAGTTCAAGAAGG	Real-time RT-PCR
For1B RT-R	GTTAGTTAGCTGCACTGCTTCC	Real-time RT-PCR
For1C RT-F	CGGAACTATCCGCAGTAAGC	Real-time RT-PCR
For1C RT-R	CTGAGCTGCTTCTACGTCTGC	Real-time RT-PCR
For1D RT-F	TCAAAGATGGAAGTCTGTGATGCG	Real-time RT-PCR
For1D RT-R	GAGTGGTGCACGCCGAGC	Real-time RT-PCR
For1E RT-F	GTCGGAATCGGAATTAGAACCACAACG	Real-time RT-PCR
For1E RT-R	TCTCGACGGTCCTGTTGATGG	Real-time RT-PCR
For1F RT-F	GGAGTGGAGGTTAAAGTCAAGG	Real-time RT-PCR
For1F RT-R	TACCTCCCTTCACAGGTTGC	Real-time RT-PCR
For2A RT-F	CACCCCTTCAAGTCACTTATCTCTGGGG	Real-time RT-PCR
For2A RT-R	TAACGGATCCGATCACCACAAGGTTCCAAATGC	Real-time RT-PCR
For2A RT-F	CACCGGATCCCCTCCAAAACACGTCTCTGAAAGG	Real-time RT-PCR
For2A RT-R	TGACTAATTTCCTCTGTCAAGGTTTCC	Real-time RT-PCR
For3 RT-F	AAGGCTTGCAATCAACTAAAATCAAGTC	Real-time RT-PCR
For3 RT-R	GCAAATGGGACCATTGATTCAATAA	Real-time RT-PCR
UbiF2	ACTACCCTGAAGTTGTATAGTTCGG	Real-time RT-PCR
UbiR	CAAGTCACATTACTTCGCTGTCTAG	Real-time RT-PCR

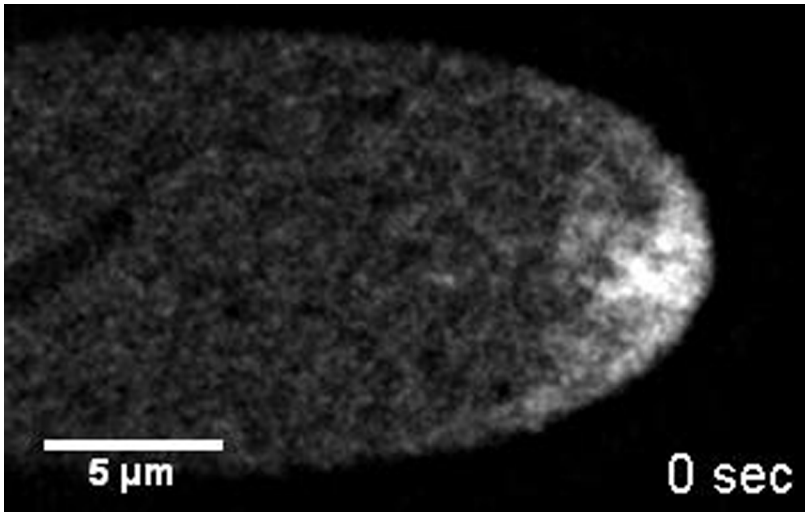

Movie S1. Functional For2A-3XmEGFP localizes to the apex of growing moss cells. Time-lapse scanning confocal microscopy of a stable line where the For2A locus was modified by integrating 3XmEGFP in frame at the 3′ end of the For2A gene. This movie contains 60 images of the medial plane of the cell taken every 20 s, and then compressed into a 6-s QuickTime movie.

Movie S1 (MOV)

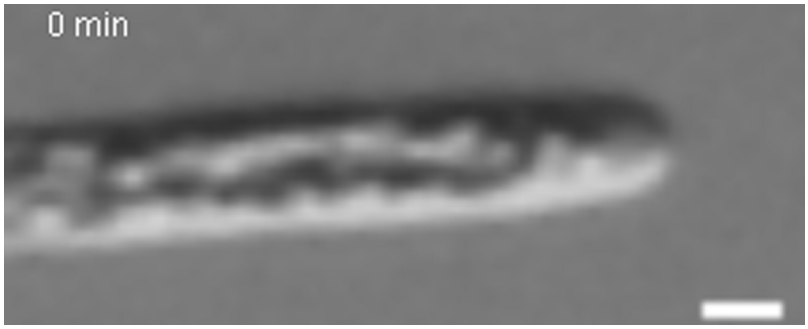

Movie S2. Time-lapse acquisition of 1-week-old control RNAi tip cell. Images were acquired with a stereo microscope at 5-min intervals using a 1× lens, zoom 63×. To display a representative sequence of a protonemal cell, a subregion was selected, interpolated, and scaled 3 times its original size. (Scale bar, 10 μm.)

Movie S2 (MOV)

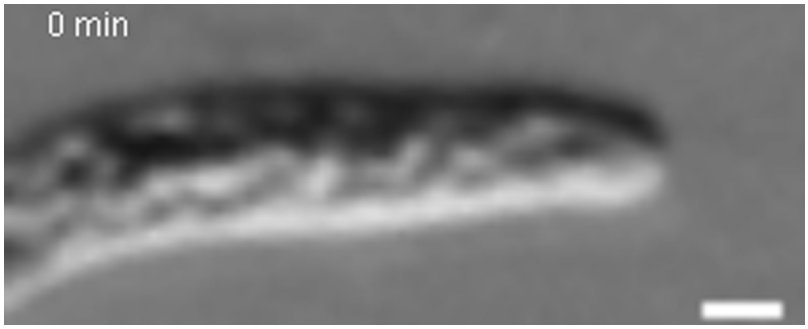

Movie S3. Time-lapse acquisition of 1-week-old class I RNAi tip cell. Images were acquired with a stereo microscope at 5-min intervals using a 1× lens, zoom 63×. To display a representative sequence of a protonemal cell, a subregion was selected, interpolated, and scaled 3 times its original size. (Scale bar, 10 μm.)

Movie S3 (MOV)

Movie S4. Profilin/alexa-532-actin polymerization in presence of For2A FH1FH2. Time-lapse TIRF microscopy of moss profilin/actin polymerization in presence of For2A FH1FH2. This movie corresponds to a large field from which the time-lapse series shown in Fig. 6 was taken. Green arrow heads indicate filaments elongating with a rate of 115 subunits/s. Red arrow heads indicate filaments that were elongating rapidly, but then stop. Yellow arrow heads indicate filaments elongating without formin associated at the barbed end, at a rate of 6 subunits/s. Images were taken every 10 s for the indicated time, and then compressed into a 10 frames per second QuickTime movie.

Movie S4 (MOV)

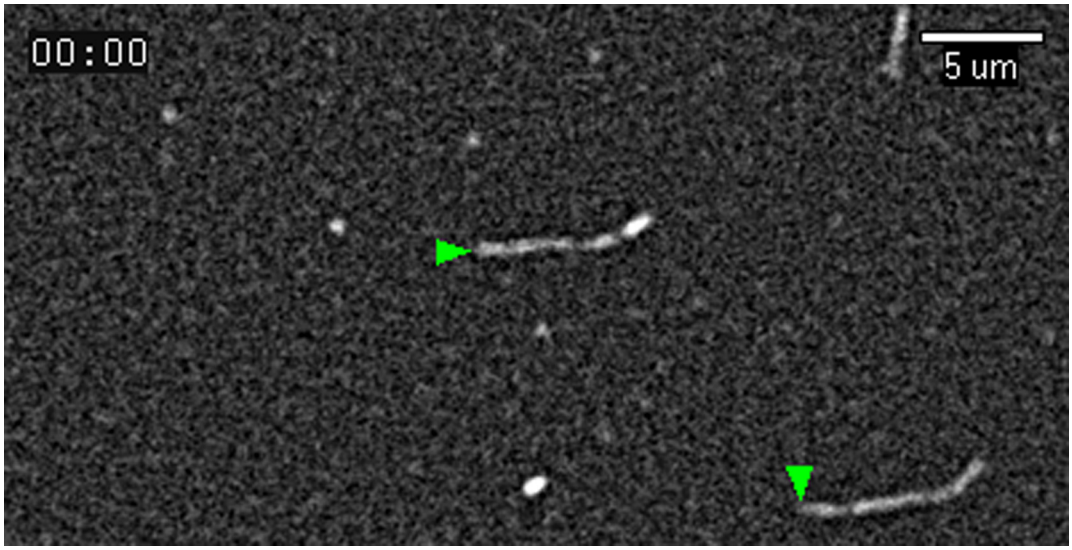

Movie S5. Profilin/Alexa-532-actin polymerization in presence of For1D FH1FH2. Time-lapse TIRF microscopy of moss profilin/actin polymerization in presence of For1D FH1FH2. This movie corresponds to a large field from which the time-lapse series shown in Fig. 6 was taken. Green arrow heads indicate filaments elongating with a rate of 24 subunits/s. Red arrow heads indicate filaments that were elongating with a For1D bound, but then stop. Yellow arrow heads indicate filaments elongating without formin associated at the barbed end, at a rate of 6 subunits/s. Images were taken every 15 s for the indicated time, and then compressed into a 6.6 frames per second QuickTime movie.

Movie S5 (MOV)

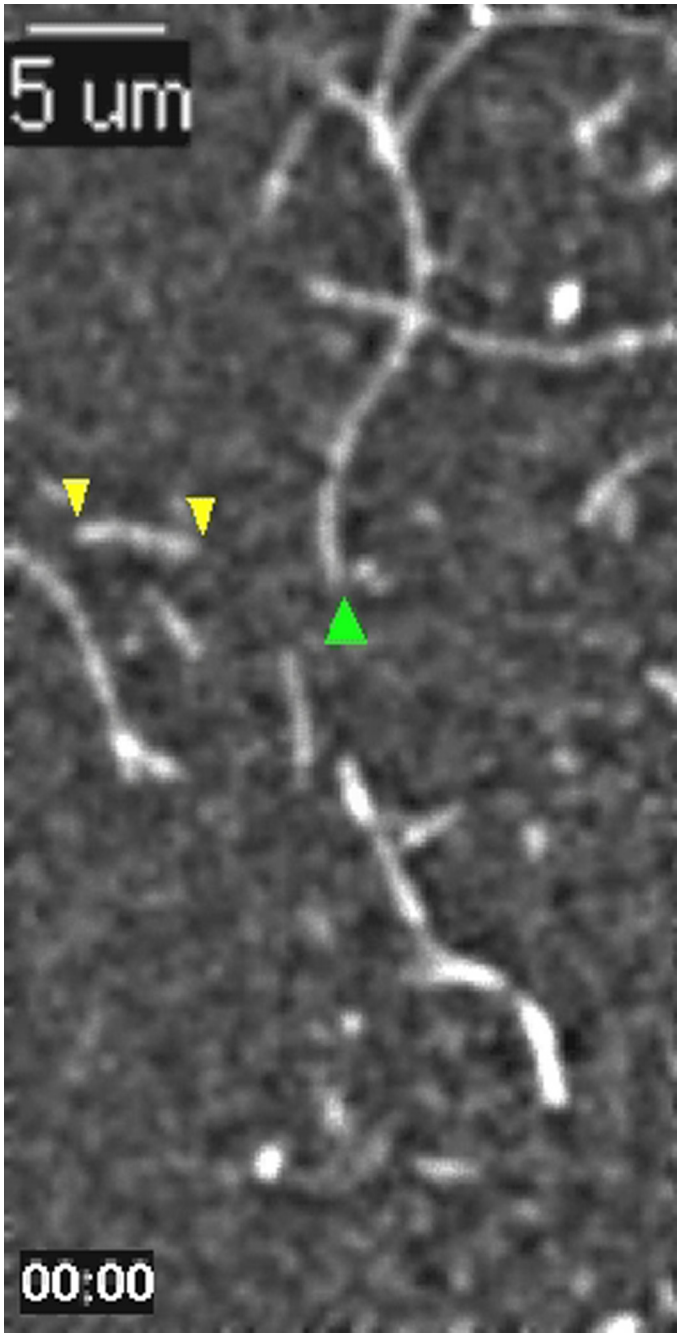

Movie S6. Profilin/Alexa-568-actin polymerization in presence of Chim1-2. Time-lapse TIRF microscopy of moss profilin/actin polymerization in presence of Chim1-2. This movie corresponds to the time-lapse series shown in Fig. 6. Green arrow heads indicate filaments elongating with a rate of 43 subunits/s. Yellow arrow heads indicate filaments elongating without formin associated at the barbed end, at a rate of 6 subunits/s. Images were taken every 10 s for the indicated time, and then compressed into a 10 frames per second QuickTime movie.

Movie S6 (MOV)

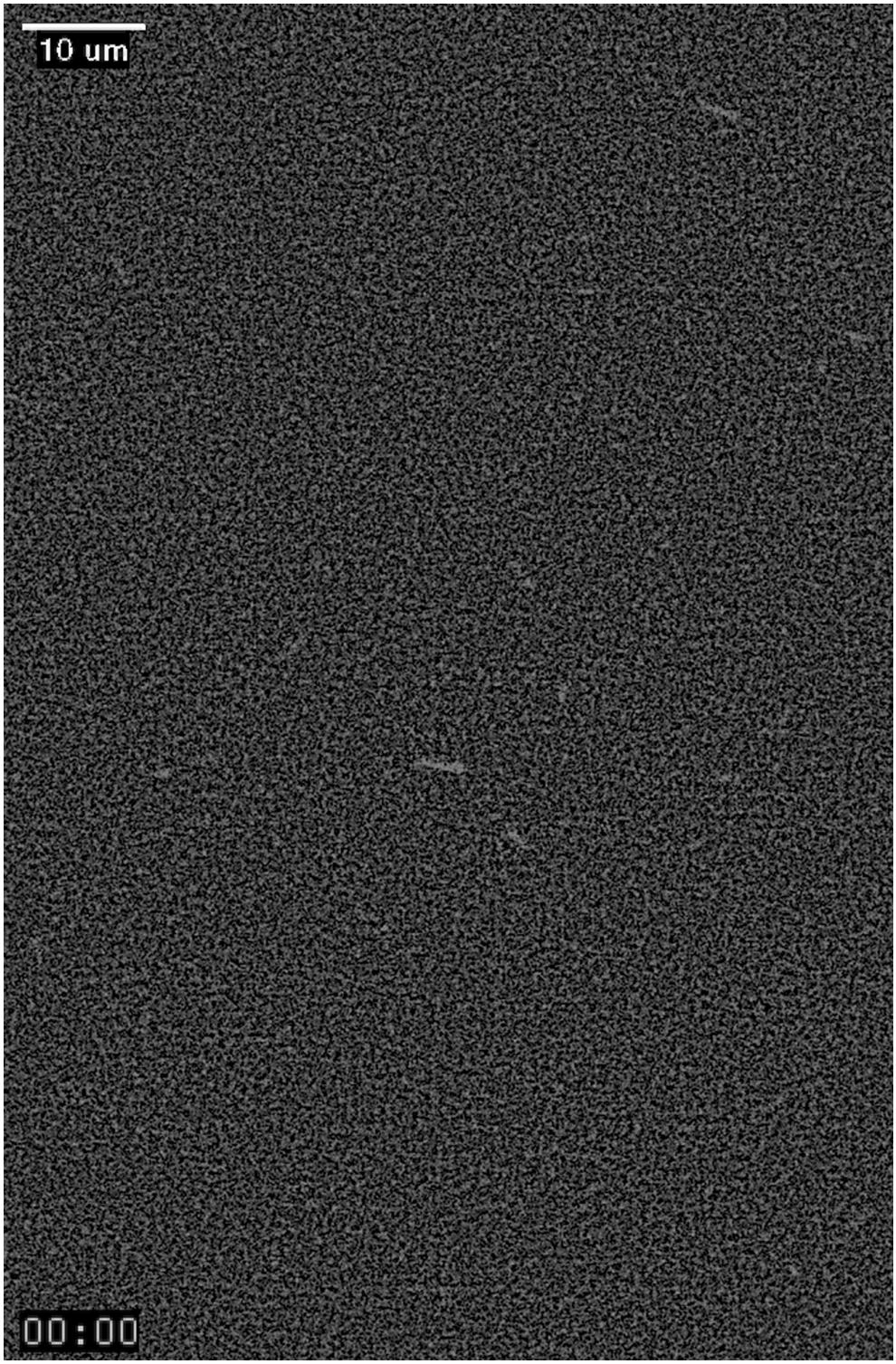

Movie S7. Profilin/Alexa Fluor 568-actin polymerization in presence of Chim2-1. Time-lapse TIRF microscopy of moss profilin/actin polymerization in presence of Chim2-1. This movie corresponds to a large field from which the time-lapse series shown in Fig. 6 was taken. Images were taken every minute for the indicated time and then compressed into a 1.6 frames per second QuickTime movie.

Movie S7 (MOV)

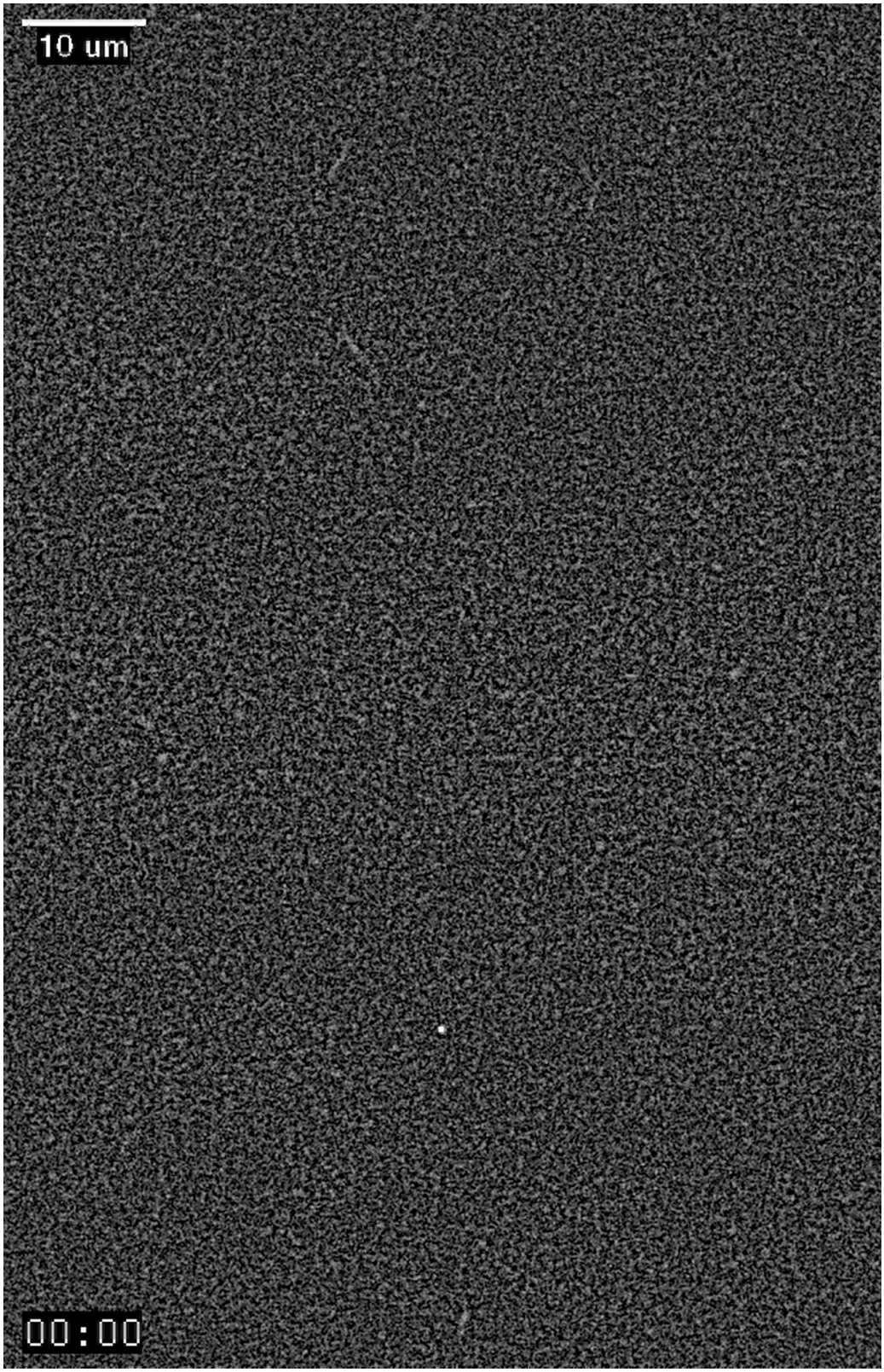

Movie S8. Profilin/Alexa Fluor 568-actin polymerization without any formin present. Time-lapse TIRF microscopy of moss profilin/actin polymerization. Images were taken every minute for the indicated time, and then compressed into a 1.6 frames per second QuickTime movie.

Movie S8 (MOV)